Continuous Photo-Oxidation in a Vortex Reactor: Efficient Operations using Air Drawn from the Laboratory

Darren S. Lee,[a] Zacharias Amara,[a] Charlotte A. Clark,[a] Zeyuan Xu,[b] Bruce Kakimpa,[b] Herve P. Morvan,[b] Stephen J. Pickering,[b] Martyn Poliakoff,[*a] and Michael W. George[*a,c]

[a]School of Chemistry, University of Nottingham, University Park, Nottingham, NG7 2RD, UK.
[b]Department of Mechanical, Materials and Manufacturing Engineering, University of Nottingham, University Park, Nottingham NG7 2RD, UK.
[c]Department of Chemical and Environmental Engineering, University of Nottingham Ningbo China, 199 Taikang East Road, Ningbo 315100, China.

Email: mike.george@nottingham.ac.uk, martyn.poliakoff@nottingham.ac.uk.

Electronic Supporting Information

Table of Contents

1. Design of the Continuous Photo-Oxidation Vortex Reactor

Our continuous photo-oxidation reactor was designed to have strong mixing and shear to increase the exposure of the reactants to the light and to promote self-cleaning of the reactor walls. A vortex reactor was chosen in which the reactor is an annular space between two cylinders. When the inner cylinder rotates, a series of toroidal vortices are formed. These are known as Taylor vortices as first observed and studied in 1923 by Taylor.[1]

Flow between two concentric cylindrical surfaces where one or both of the cylindrical surfaces is or are rotating is laminar flow when the rotating speed is low and is known as rotating Couette flow. When the rotating speed is increased, the flow becomes unstable if the angular velocity exceeds a critical value and a steady axisymmetric secondary flow in the form of regularly spaced toroidal vortices is generated. This is known as Taylor-Couette flow. Alternate vortices rotate in opposite directions and generate a complex toroidal vortex pattern in the gap. The stability of flow depends on the rotating speed of cylinder, fluid properties and geometry of the annulus. For the case of a stationary outer cylinder and a rotating inner cylinder, the critical value of the dimensionless Taylor number[2] (*Ta*) where vortices are generated (for an annulus width that is small compared to the inner radius) in the flow is given by:

$$Ta = \frac{r_i (r_0 - r_i)^3 \Omega_i^2}{\upsilon^2} \approx 1700$$

The Taylor number is a dimensionless number based on these parameters, where r_i, r_o, and Ω_i are the radius of inner surface, outer surface, and rotational speed of inner surface respectively, as shown in Figure S1. While v is the kinematic viscosity of fluid in the gap between two surfaces.

Further increasing the rotational speed, many regular flow configurations can exist beyond the first transition to Taylor vortex flow; these flow configurations are generally called wavy vortex flow. They are characterized by a pattern of traveling waves, which are periodic in the circumferential direction and appear just above the critical Taylor number. It is found that the presence of an axial flow will tend to suppress the formation of the Taylor vortices and would therefore reduce the mixing. However, at the flow rates used in this investigation the axial velocity is very low relative to the rotational speed and so any effect would not be noticed.

.

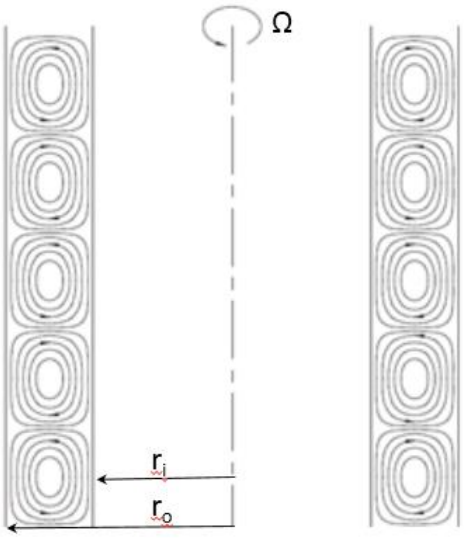

Figure S1. A typical Taylor vortex flow

Taylor vortex flow theory can be applied to design the vortex reactor to generate a wavy vortex flow in the gap between the two cylindrical surfaces. If the outer cylinder is transparent the reactants in the annular gap can be irradiated with light and the vortices will provide a rapid mixing in the flow refreshing the reactants exposed to the light close to the outer cylinder. The strong shear over the outer cylinder surface also helps to keep the surface clean.

The concept of reactor is shown in Figure S2 and consists of a stationary outer tube and rotating inner tube. The outer tube is made of glass to allow light to be introduced. Fluid is continuously introduced from a central tube within the rotating tube and exits the reactor from top edge of the annulus gap. Air is sucked into the reactor from the free surface at the top of the annulus gap when the inner tube is rotating due a negative pressure that is generated near the inner rotating surface by the centrifugal force in the rotating fluid region.

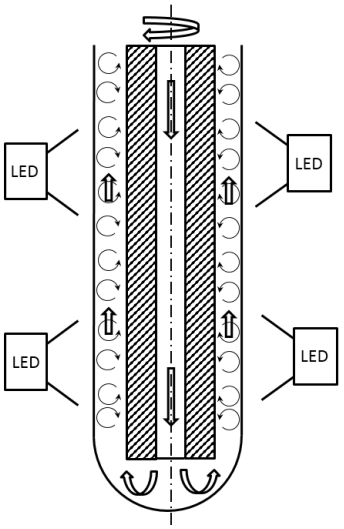

Figure S2. The vortex reactor concept

A simple test rig was used to investigate the shaft diameter. A common chemical glass test tube, 20 mm diameter, was selected for the outer stationary tube whilst the inner rotating tube was made of stainless steel to give a high shaft stiffness. The gap between the surfaces was then controlled by changing the diameter of inner rotating shaft. Figure S3 shows how the Taylor number varied with the inner diameter of rotating shaft for a fixed outer tube of 20 mm. As the gap is increased, the flow becomes less stable at the same rotating speed and the critical Taylor value occurs at lower rotating speed. A shaft diameter of 18 mm was selected for the final reactor design.

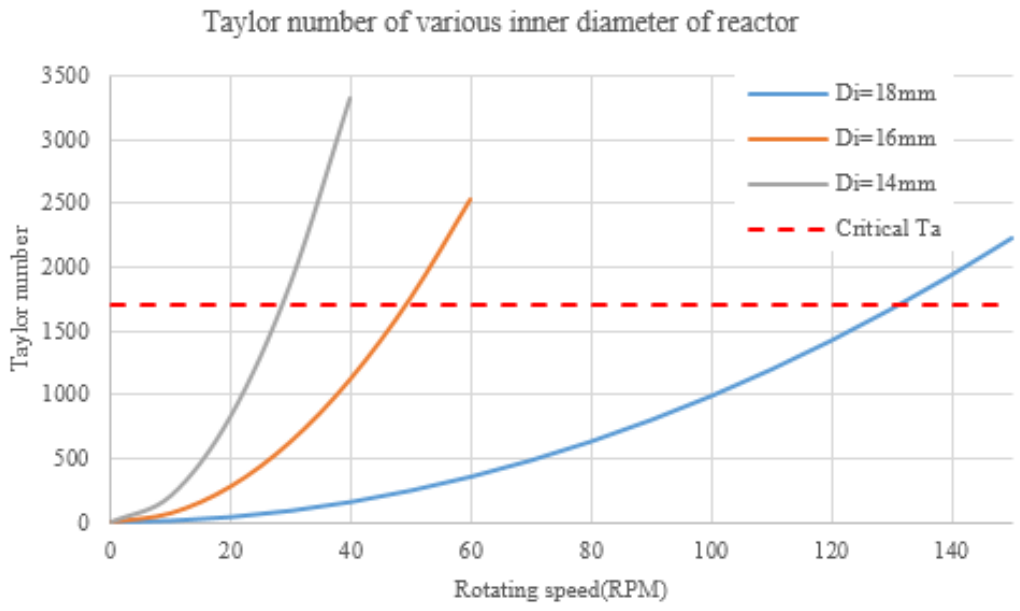

Figure S3. Critical Ta number of various rotating shaft diameters use water as fluid.

The reactor was designed as described above and is shown in Figure S4. A speed controlled motor drives the inner tube through a belt at top of the test section, the rotating speed of the inner tube can be controlled continuously from 0 to 4000 rpm which corresponds to a Taylor number of $4x10^7$ at the top speed if water is used as working fluid. This is well into the flow regime where Taylor vortices are formed. The inner shaft was also designed to be rotationally stable at the operating speeds and it only operates at about 10% of the critical rotational speed.

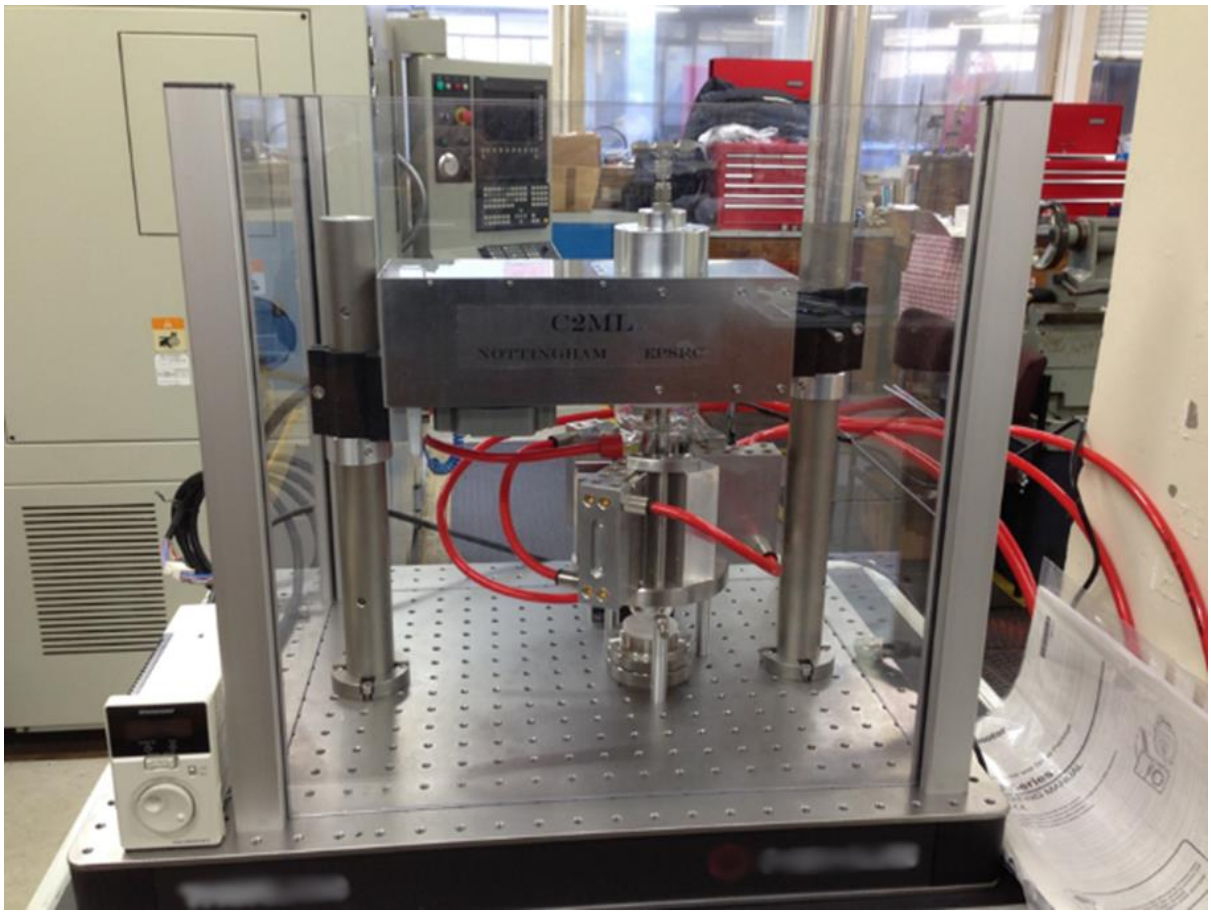

Figure S4. Continuous Photo-Oxidation Vortex Reactor

2. Computation Fluid Dynamics (CFD)

Computational Fluid Dynamics (CFD) were used to visualise the flow pattern in the reactor. Commercial CFD software Ansys Fluent[3] was used for flow simulation of the reactor in 3D. In order to save the computational time, only 20 degree of test section was simulated with cylindrical periodic boundary conditions. Figure S5a shows the computational domain of the CFD and the Navier–Stokes equations control flow is solved numerically in the cylindrical computational domain. The turbulent properties distributions with flow are simulated using k-ε model with enhance wall function in the region near the wall.

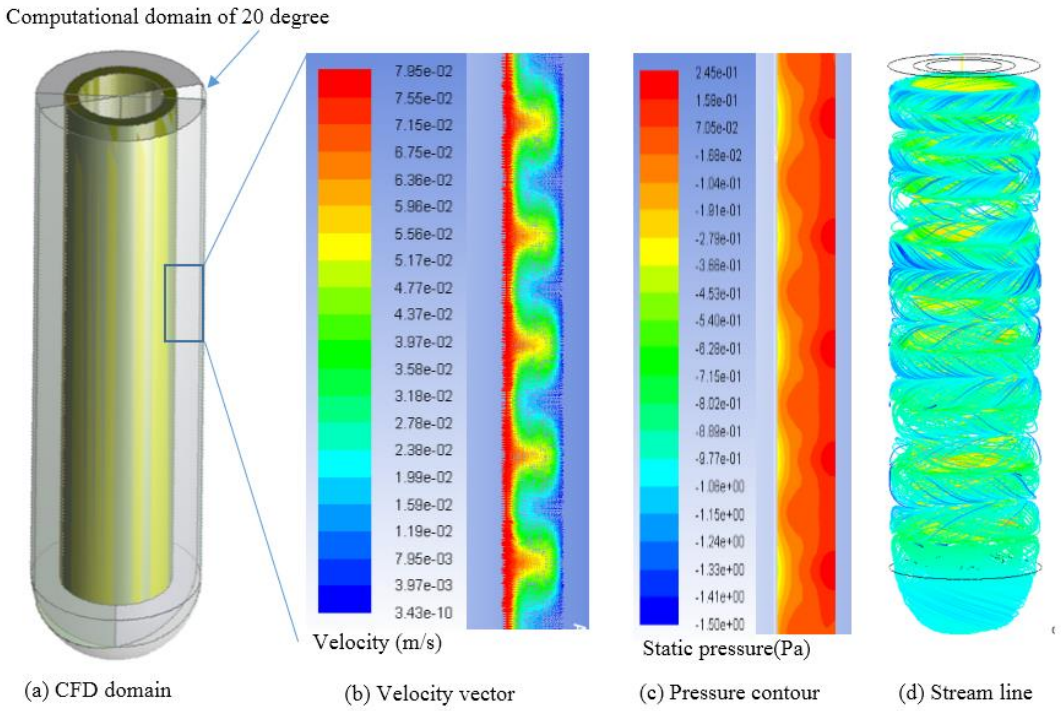

Figure S5. (a) Computational domain **(b)** Velocity distribution in the annulus gap at angular speed of 10rad/s **(c)** Pressure contours in the annulus gap at angular speed of 10rad/s **(d)** Flow streamlines.

Figure S5b-c illustrates the CFD results for a rotating speed of 10 rad/s of the inner tube. A high speed region of velocity occurs near the rotating surface of inner tube and paired vortices are generated periodically in the annular gap. The pressure contours in the corresponding region are shown in Figure S5c, where a negative pressure region is generated near the inner rotating wall. A pressure gradient is built up across the annulus gap with a negative pressure near inner surface where air is sucked into the reactor as observed by bubbles during experiments. The flow streamlines are shown in Figure S5d, toroidal vortices can be seen in the figure which also helps bring the air bubbles down in to the annulus gap to mix with the fluid within the gap.

The velocity plots show that the strength of the vortices gives radial and axial velocities in the vortices that are typically 10%-20% of the peripheral speed of the inner rotor. The vortices are approximately circular in the axial/radial plane and thus provide a significant convective mass transfer across the annulus that is much greater than would be achieved by diffusion alone in a purely annular flow. The vortices also provide greater shear over the outer walls of the annulus, which would help to keep them clean. Future research will include development of the CFD modelling to include the photochemical reactions and effect of the second phase. This will then allow scale up to be modelled with greater confidence.

3. Dissolved oxygen studies

It has been shown previously that pyrogallol dissolved in basic solution can act as a reporter as to the amount of dissolved oxygen.[4,5] This can be measured by UV-Vis absorption spectroscopy as the starting colourless solution changes colour on exposure to oxygen. We sought to use this reaction as a system for determining the effect of rotation speed on the oxidation of a pyrogallol solution and hence to act as an indicator for the amount of dissolved oxygen under the different spin speeds.

A 200 mL aqueous solution containing $NaHCO_3$ (0.2 g, 2 mmol) was prepared using standard Schlenk techniques and thoroughly degassed by bubbling Argon through the solution. Transfer of this solution to another vessel containing the pyrogallol (80 mg, 0.63 mmol) was performed using a cannula under an Argon atmosphere. Measurement of absorption spectra were obtained using a Agilent 8453 spectrometer using a solution flow cell (Harrick Scientific products Inc.) fitted with CaF_2 windows attached to the output of the peristaltic pump. The flow rates of the solution and peristaltic pumps remained fixed at 1.0 mL min^{-1} and 50 rpm respectively. Three full reactor volumes were passed before spectra were recorded to ensure that the output of the reactor had reached a steady state. Multiple spectra were recorded and averaged at each rotation speed.

4. Experimental Methods and Spectra

General Information

All solvents and reagents were used as obtained without any further purification. Phenyl boronic acid was recrystallised from H_2O prior to use. Furfural was distilled over 4Å MS prior to use. Proton (^1H) NMR spectra were recorded with a Bruker DPX300 spectrometer at ambient temperatures unless otherwise specified. Chemical shift values are reported in ppm, and solvent resonances were used as internal standards ($CHCl_3$: δ = 7.26 ppm for ^1H). Biphenyl was used an internal standard for determining the yields and/or conversion of **2** and **8**. For the yield/conversion of **5** and **7**, 1,3,5-trimethoxybenzene was used as an internal standard. The spectra were assigned comparing chemical shifts to existing literature values and commercial samples.

General Reactor Operation

The LED recirculating chiller was turned on and set to 5 °C whilst the reactor chiller was set to the appropriate temperature for the reaction. The chillers were left to equilibrate for ca. 20 min. The reaction mixture was prepared as described below and the inlet pipe for the HPLC pump was fed into the solution and the pump primed. The desired flow rate was set on the HPLC pump and the solution pumped. The peristaltic pump to remove the products from the reactor was set to 50 rpm. The rotation motor was turned on and slowly increased until the desired rotation speed was achieved. Then the LEDs were turned on at full brightness. Two full reactor volumes were allowed to pass before taking a sample for analysis, this ensured that the reactor had reached a steady state.

Once the operation was complete, the LEDs and the HPLC pump were turned off, and the rotation motor was slowly decreased to 0 rpm. The recirculating chillers were also turned off, providing the LED blocks were not excessively hot. The inlet pipe was switched to a container with a compatible solvent (usually the reaction solvent) and the reactor was flushed at 2-5 mL min^{-1}**.** The rotation speed was set to 200 rpm during this time and increased to 4000 rpm occasionally to ensure that all material was removed from the reactor. Once the reactor was clean, the motor and pumps were turned off.

Photo-oxidation of α-terpinene 1 to ascaridole 2.[6]

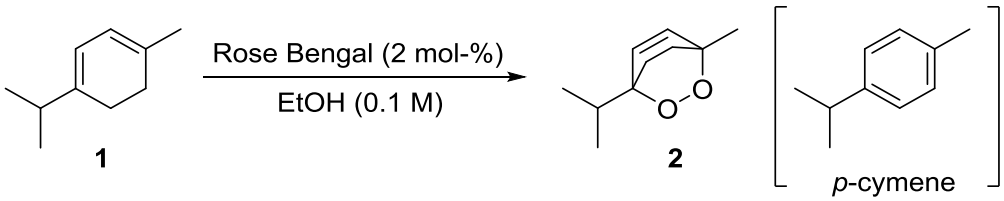

Representative ^{1}H NMR spectra for the conversion of α-terpinene (**1**) to ascaridole (**2**) in the vortex reactor.

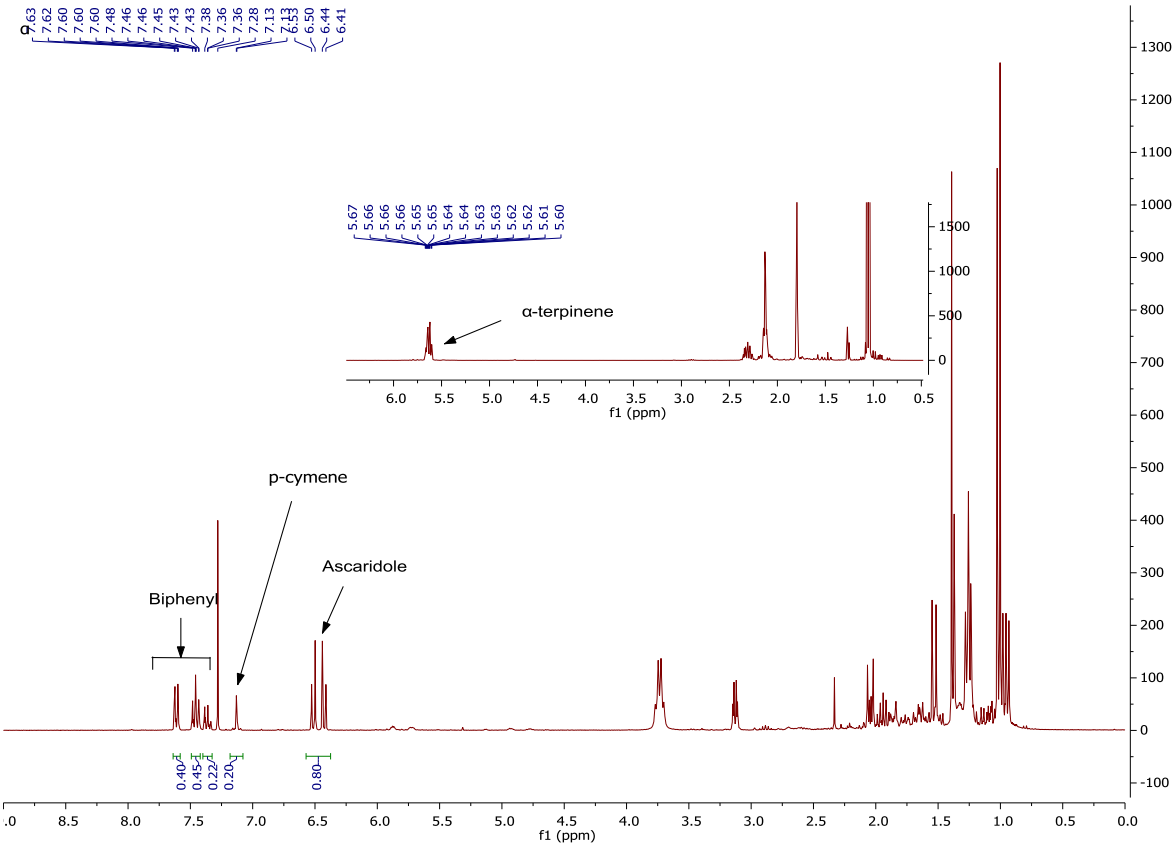

Photo-oxidation of furfural 4 to 5-hydroxyfuran-2(5H)-one 5.[7]

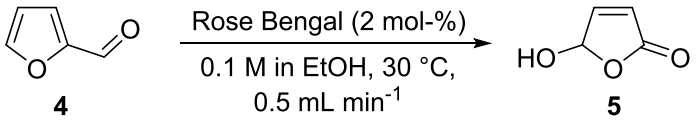

4 **5**

Representative ^{1}H NMR spectra for the conversion of furfural (**4**) to 5-hydroxyfuran-2(5H)-one (**5**) in the vortex reactor.

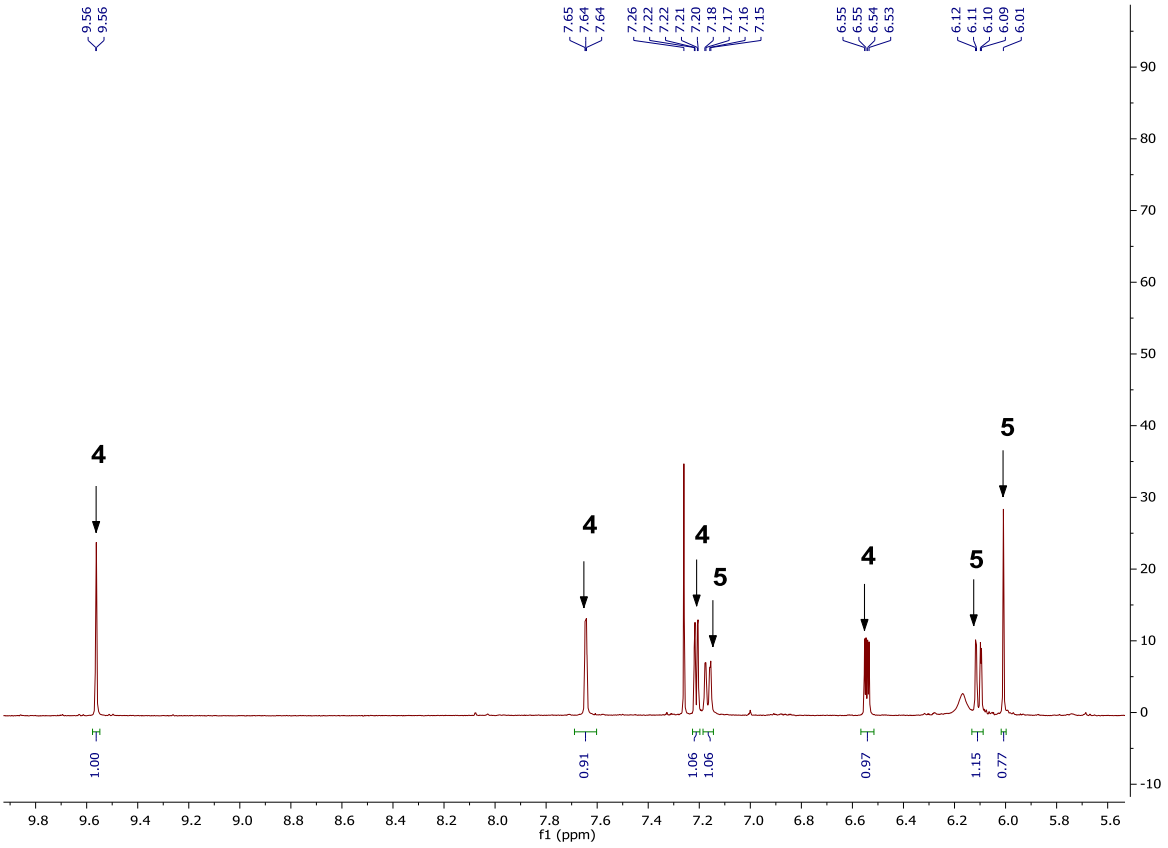

Photodeborylation of phenyl boronic acid 6 to phenol 7.[6,8]

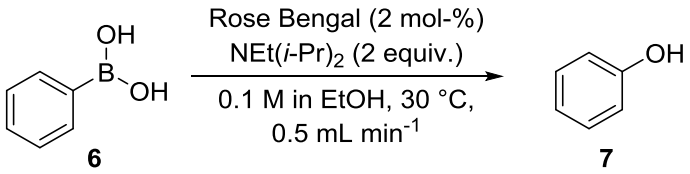

Representative ^{1}H NMR spectra for the conversion of phenylboronic acid (**6**) to phenol (**7**) in the vortex reactor.

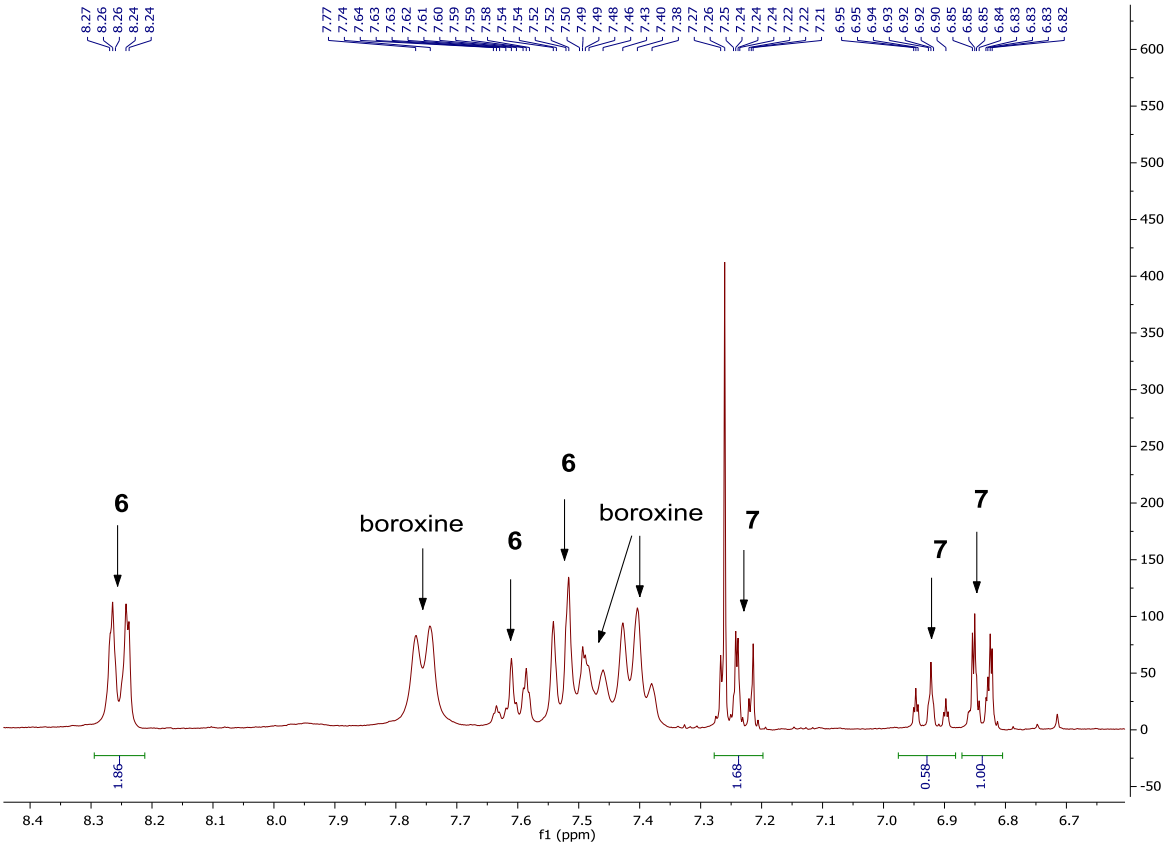

Photo-oxidation of DHAA 9 to Artemisinin 8.[9]

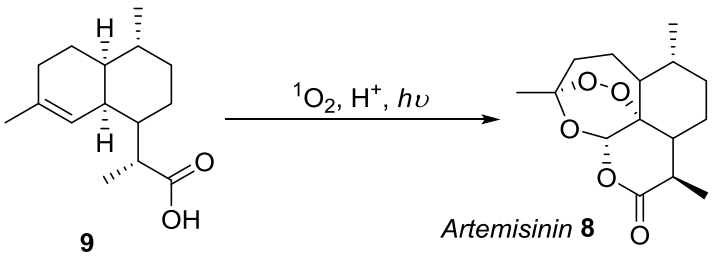

Representative ^{1}H NMR spectra for the conversion of DHAA (**9**) to artemisinin (**8**) in the vortex reactor.

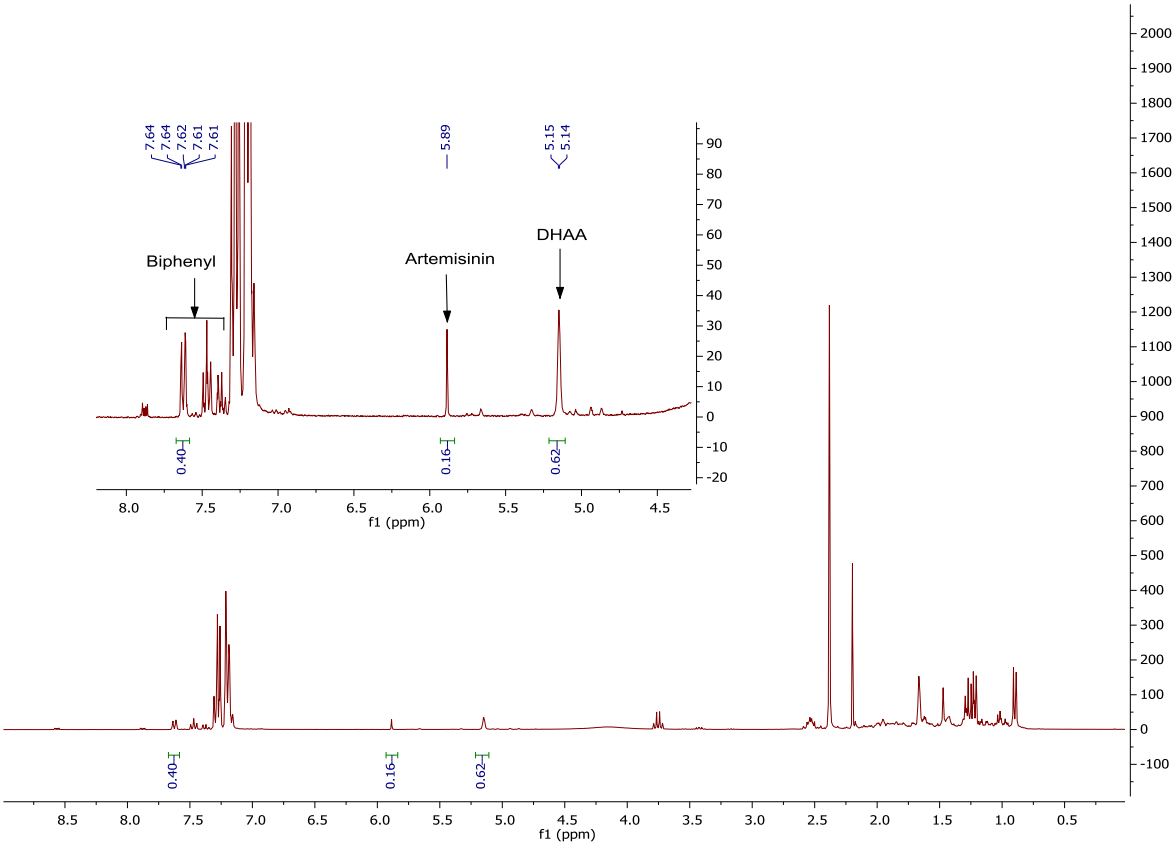

5. References

1. Taylor, G. I. *Phil. Trans. Roy. Soc. London Ser. A*, **1923**, *223*, 289-343.
2. White, F. Fluid Mechanics, **2015**, McGraw-Hill Education
3. http://www.ansys.com/Products/Fluids/ANSYS-Fluent
4. Williams, D. D.; Blachly, C. H.; Miller, R. R. *Anal Chem* **1952**, *24*, 1819.
5. Duncan, I. A.; Harriman, A.; Porter, G. *Anal Chem* **1979**, *51*, 2206.
6. Clark, C. A.; Lee, D. S.; Pickering, S. J.; Poliakoff, M.; George, M. W. *Org. Process Res. Dev.* **2016**, *20*, 1792-1798.
7. Morita, Y.; Tokuyama, H.; Fukuyama, T. *Org. Lett.* **2005** *7*, 4337-4340.
8. Penders, I. G. T. M.; Amara, Z.; Horvath, R.; Rossen, K.; Poliakoff, M.; George, M. W. *RSC Adv.* **2015**, *5*, 6501-6504.
9. Amara, Z.; Bellamy, J. F. B.; Horvath, R.; Miller, S. J.; Beeby, A.; Burgard, A.; Rossen, K.; Poliakoff, M.; George, M. W. *Nat. Chem.* **2015**, *7*, 489-495.